



Application of computed tomography in the analysis of glass beads unearthed in Shanpula cemetery (Khotan), Xinjiang Uyghur Autonomous Region

Qian Cheng¹ · Xueyan Zhang² · Jinlong Guo³ · Bo Wang³ · Yong Lei² · Guangzhao Zhou⁴ · Ya'nan Fu⁴

Received: 14 August 2017 / Accepted: 28 November 2017 / Published online: 13 December 2017
© Springer-Verlag GmbH Germany, part of Springer Nature 2017

Abstract

The glass beads unearthed in sites along the Silk Road usually indicate the communications of arts, business, and cultures between different areas. The production process of glass beads also implies an associated local culture, as well as its provenance. Computed tomography (CT) is a non-destructive three-dimensional method and it has been widely used in the research of various relics. It contributes to discovering and documenting the manufacturing processes for artifacts. Based on the CT images of two glass beads which were unearthed in Khotan, Xinjiang, China, the inner structure and air bubble shapes were investigated. This paper demonstrates how the CT technology contributes to studying the manufacture of archaeological glass beads. Two polychrome beads were analyzed by CT scanning techniques. Bead S-2 is a typical natron glass and bead SC-8 is a soda-lime-silica glass, based on the chemical components analyzed by laser ablation inductively coupled plasma atomic emission spectrometry (LA-ICP-AES). According to computed tomographic analysis, a porous core was covered with a thick layer of glaze. The eye parts from S-2 eye bead were probably made by an embedding technique, which was proved by the 3D shapes of bubbles and the “eyes.” The SC-8 bead was manufactured by a stretching technique which was evidenced by the elliptical bubbles. The yellow stripes wrapped around the glass base present sharp edges in cross section, which seem to reflect grooves carved before the filling process.

Keywords Computered tomography · Glass beads · Silk Road · Glass-working technique

Introduction

The Silk Road was a famous and historic route representing economical, cultural, and aesthetic exchanges between the East and West. The Silk Road route was divided into three ways in the Xinjiang region (the north way, the middle way,

and the south way). The north way is from Anxi to Almaty via Hami, Turfan. The other two divided in Dunhuang and circumvented the Taklamakan Desert. The middle way went through Loulan, Aksu, and the south one went through Khotan. Then, they rejoined at Kashgar (Ferdinand von Richthofen 1877:454; Meicun 2006:1e4), as shown in Fig. 1.

The Xinjiang region was a historic trade and cultural hub between the world of East and West. Study of the relics excavated in this region has been an important topic in worldwide historical and archeological scholar. Glassware is particularly unique and colorful among the various ancient objects made by traditional craftsmen. The Lop County, on the south route of the Silk Road and located in the Hetian Oasis in the southern Tarim Basin of Xinjiang, China, was the main activity zone of the Khotan residents. The Shanpula cemetery site is about 14 km to the southwest of Lop County and is regarded as one of the most important archaeological discoveries in Xinjiang since the 1980s (Fig. 1). A huge number of precious

✉ Yong Lei
leiyongleo@hotmail.com

✉ Guangzhao Zhou
zhouguangzhao@sinap.ac.cn

¹ Chinese Academy of Cultural Heritage, Beijing, China

² Conservation Department, The Palace Museum, Beijing, China

³ Museum of Xinjiang Uyghur Autonomous Region, Urumchi, China

⁴ Shanghai Synchrotron Radiation Facility, Shanghai Institute of Applied Physics, Chinese Academy of Sciences, Shanghai, China



Fig. 1 The ancient Silk Road map, the Shanpula tomb site in Khotan was circled

archaeological finds such as ironware, wooden objects, pottery, textiles, and glass have been unearthed there.

More than 2000 glass finds were unearthed from the Shanpula cemetery; they were mainly in the form of glass beads strung into necklaces, bracelets, and earrings, mixed with stone and bone beads. Those beads can be classified in terms of color and pattern of decoration.

Those beads can be classified as three assortments in terms of appearance: monochrome bead, dragonfly eye bead, and dual-color beads (Xinjiang Uygur Autonomous Region Museum 2001). There are 47 samples including 42 monochrome beads and 5 polychrome beads which have been chosen to represent the about 2000 archeological glass beads according to color and decoration pattern. The chemical compositions of samples were analyzed by laser ablation inductively coupled plasma atomic emission spectrometry (LA-ICP-AES), employing the Corning glass B standard as a quantitative controlling reference glass (Qian 2017).

Normally, when studying integral glass finds in good condition, we only obtain information from their surfaces, such as type, color, and weathering. It is more difficult to understand their inner structure or chemical composition without polishing or breaking. Since these museum collections have

to be managed under strict regulations, they are required to be well-stored and guarded from any damage. Thus, researchers are encouraged to obtain relevant information by using non-destructive methods. Fortunately, the CT technology, a non-destructive method, has been widely applied in the field of archaeology.

The advantage of CT technology is detecting the interior structure of a sample without any degradation. By X-ray irradiation, the detectors acquire the signal that penetrates the samples. The “density differences” produce the different gray levels in the CT images. With the filtered back projection (FBP) algorithm, the geometric structure and interior information of the samples can be determined.

In this paper, the authors focus on the application of CT techniques on archaeological glass finds, because much more potential information could be investigated from polychrome rather than monochrome beads. There are two samples, one is an eye bead and another one is a blue bead with stripe pattern, embody 5 polychrome beads. Both of them were discovered from the Shanpula cemetery and collected in the Museum of the Xinjiang Uygur Autonomous Region. By using CT scanner, we explored the samples and obtained some unexpected results which could not acquire by other methods for surface analysis.

Materials and methods

Synchrotron radiation X-ray micro-tomography

The luminous flux output of synchrotron radiation sources in phase-contrast CT is tens of thousands of times. Propagation-based phase-contrast imaging can distinguish the boundary of different materials especially low-Z materials. Phase retrieval enhances the contrast of different materials (Ren Yuqi et al. 2013:762e765; Baruchel et al. 2006:41e46). Moreover, synchrotron radiation sources can generate continuous spectrum X-rays, and monochromatic X-rays of particular energies could be produced by monochromator.

The installation picture of BL13W1 of the Shanghai Synchrotron Radiation Facility is as shown in Fig. 2. The energy of BL13W1 covered 8.0–72.5 keV with the gap 17–35 mm. A Si (111) crystal and a Si (311) crystal were combined with the double monochromator crystal. The resolution of three directions (X, Y, Z) is all of $> 1 \mu\text{m}$. This station could achieve its imaging function either by absorption-contrast imaging or phase-contrast imaging mechanism. Technologies including 3D reconstruction of high resolution, by which the 3D micro CT imaging of high resolution can be achieved.

Within traditional archaeological and archaeometric fields, researches on glass beads mostly focus on the origin, manufacture, and aesthetics by analyzing the similarity and difference in terms of the patterns, colors, and chemical components, but only focus on the physical structure. In this research, the interior features of the unearthed glass beads and oval beads have been measured by synchrotron-based X-ray computed micro-tomography (SR- μCT) at BL13W1 of Shanghai Synchrotron Radiation Facility (SSRF). The SR- μCT technique has been widely used in the field of materials, archaeology, biomedicines, and geosciences (Shijie et al. 2013:195e196; Tafforeau et al. 2006:195e196; Jensen et al. 2011:1718e 1720; Betz et al. 2007:59e66).

Background of the samples

In this paper, two glass beads, S-2 and SC-8, from the Shanpula cemetery were selected for CT scanning analysis.

S-2 is a round eye bead which made in white monochrome base glass decorated with multi-color spots in the form of eyes. One opaque white and yellow concentric circles, plus a dark blue pupil, comprise one eye. The six eyes were embedded in the bead (Fig. 3). S-2 is an archaeological find bead from tomb No. 35 which was dated between the middle of the third century AD and the end of the fourth century AD. The size is 10.52–10.83 mm (external diameter), 4.0 mm (bore diameter), and 7.35 mm (height). SC-8 sample is a bi-color bead with blue ground embedded with yellow curved stripes. The size is 10.32 mm (external diameter), 2.37 mm (bore diameter), and 21.37 mm (height). This bead was made in a spindle shape and is illustrated in Fig. 3. The bead was picked up from the ground surface due to a flood which occurred in area of the tomb site. SC-8 has been dated to the first century BCE to the end of the fourth century CE according to the archaeological report (Xinjiang Museum 2001).

These two samples have been analyzed by LA-ICP-AES. By ablating the weathered layer of the sample to a certain depth, a fresh layer was exposed producing reliable data. The detection limit for the glass analysis by this method can satisfy a value of 0.0001%. The Corning glass B standard was also employed as a quantitative controlling reference glass (Vicenzi et al. 2002). The results of chemical composition have been listed in Table 1, and measurement parameters of the instrument have been listed in Table 2.

According to the chemical composition of sample S-2, SiO_2 is 56.61%, Na_2O 12.7%, and CaO 4.42%; the impurity elements MgO and K_2O are quite low, 0.75% and 0.83%, respectively. Chemical composition of the eye part in dark blue and yellow color shows that MgO and K_2O are lower than 1%. Therefore, the eye bead S-2 is a typical low-magnesium-potassium (LMLK) natron glass bead of Roman period, whose fluxing agent is natron or evaporation salt (Cheng Qian, unpublished report; Laure and Bernard 2013:399e411) (Table 1). In the white opaque glass with very high Sb_2O_3 9.86%, analysis indicates the opacifier could be $\text{Ca}_2\text{Sb}_2\text{O}_7$.

In the Roman Period, many vessel, tesserae, and enamels were found to be opacified with $\text{Ca}_2\text{Sb}_2\text{O}_7$ crystals.

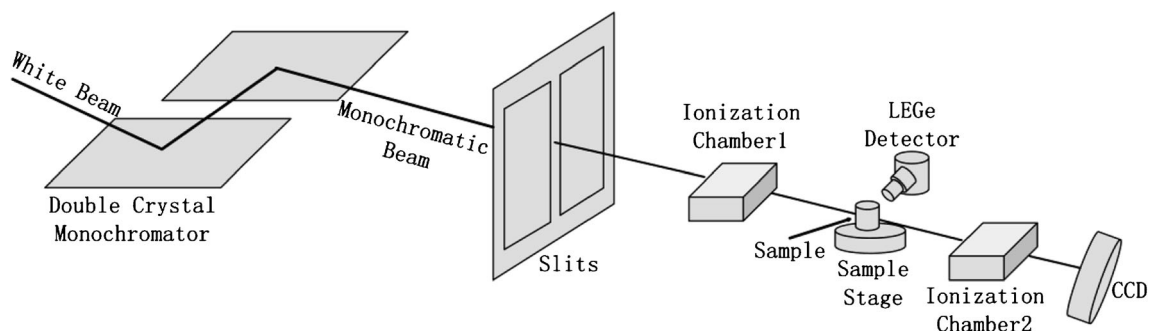
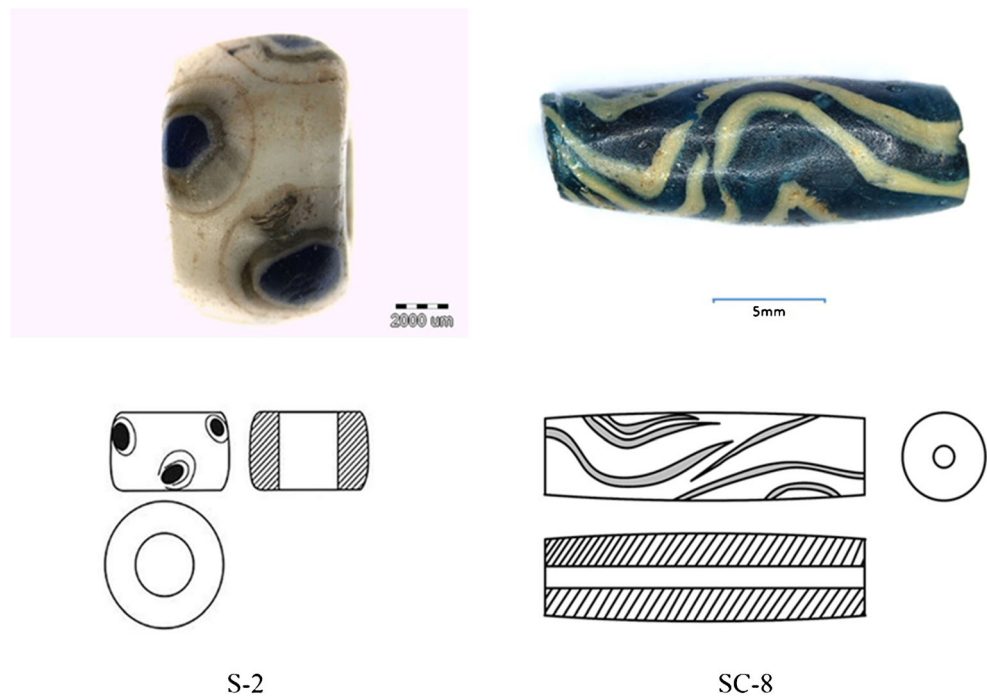


Fig. 2 The installation picture of BL13W1 of the Shanghai synchrotron radiation sources (Ren Yuqi et al. 2013:765)

Fig. 3 The photos and line drawings of samples



Henderson's study (Henderson 1991.) shows that during the first to fourth century AD, all the samples of blue, turquoise,

and green enamels were found to be opacified with $\text{Ca}_2\text{Sb}_2\text{O}_7$ crystals.

Table 1 The results of chemical compositions by LA-ICP-AES (wt.%) (Cheng 2017)

	S-2			SC-8	
	Body—white	Eye—dark blue	Eye—yellow	Body—blue	Stripe—yellow
SiO_2	56.61	70.28	77.28	59.28	52.31
Al_2O_3	1.80	1.81	2.41	5.27	4.39
Fe_2O_3	0.65	1.42	0.92	0.84	0.71
MgO	0.75	0.61	0.73	3.57	3.44
CaO	4.42	6.63	5.50	5.96	5.47
Na_2O	12.7	14.6	6.4	18.7	16.5
K_2O	0.83	0.70	1.08	4.89	4.19
MnO_2	0.83	2.38	0.18	0.08	0.07
P_2O_5	0.07	0.03	0.11	0.14	0.08
TiO_2	0.17	0.14	0.19	0.19	0.17
Sb_2O_3	9.86	0.02	2.29	0.003	0.00
CuO	0.42	1.06	0.04	0.70	0.04
PbO	10.74	0.00	2.52	0.09	11.13
CoO	0.00	0.22	0.00	0.00	0.00
BaO	0.04	0.03	0.04	0.16	0.15
SnO_2	0.07	0.02	0.18	0.01	1.27
SrO	0.04	0.04	0.03	0.06	0.06
ZnO	0.00	0.01	0.002	0.003	0.003
B_2O_3	0.03	0.012	0.03	0.06	0.05
V_2O_5	0.00	0.02	0.06	0.003	0.004
NiO	0.00	0.01	0.01	0.001	0.003
ZrO	0.01	0.01	0.01	0.01	0.01
Ag_2O	0.001	0.00	0.00	0.00	0.001

Table 2 Instrument and measurement parameters

Prodigy high dispersion ICP-AES: Leeman Labs Inc., USA	
RF generator: 40.82 MHz	RF power: 1.1KW
Argon flow rate	
Plasma: 1.4 l/min	Auxiliary pressure: 0 psig
Nebulizer pressure: 35 psig	
Laser ablation system: UP-266 Marco, New-Wave Inc. USA	
Laser: ND-YAG	Laser mode: Q-switched
Laser wavelength: 266 nm	Output energy: 10 ± 1 mJ
Facular aperture: 515 μ m	Helium flow rate: 800 ml/min

SC-8 is a typical soda-lime-silica due to the chemical composition of SiO_2 59.28%, Na_2O 18.7%, and CaO 5.96%. Relatively high MgO and K_2O in 3.57% and 4.89% reflect that plant ash, rather than natron salt, was used as flux containing a greater amount of impurity elements. In the tomb site, there are almost 20 similar beads but difference sizes were discovered and collected. This type of bead was possibly produced from the Bare site, 7 km from Peshawar city, near the ancient Pushkalavi, dated from the second century B.C. to the second century A.D. due to the slimmer appearance and chemical compositions. The yellow stripes which contain high PbO in 11.13% and SnO_2 in 1.27% reflect on the existence of lead-tin yellow colorant ($\text{Pb}_2\text{Sn}_2\text{O}_7$) (Laure and Bernard 2013:399e411).

Experiment and conditions

Phased contrast SR- μ CT was employed to capture images of the specimen at beamline BL13W1 (SSRF, Shanghai, China). The beam size was 20 mm \times 2.7 mm (H \times V) and the energy was optimized at 65 KeV (S-2) and 30 KeV (SC-8). The image voxel size was 9 μ m \times 9 μ m \times 9 μ m. The detector was positioned at 70 cm downstream of the sample. The CT scanned 1000 projections on S-2 and 720 projections on SC-8

Fig. 4 The different slices of S-2 (the distinct colors represent the different materials. **a** The cross-section slice of S-2. The arrow shows the direction of stress, which is perpendicular to the long axis of the oval bubbles. **b** The longitudinal section of S-2. The white line shows the boundary between the two similar materials

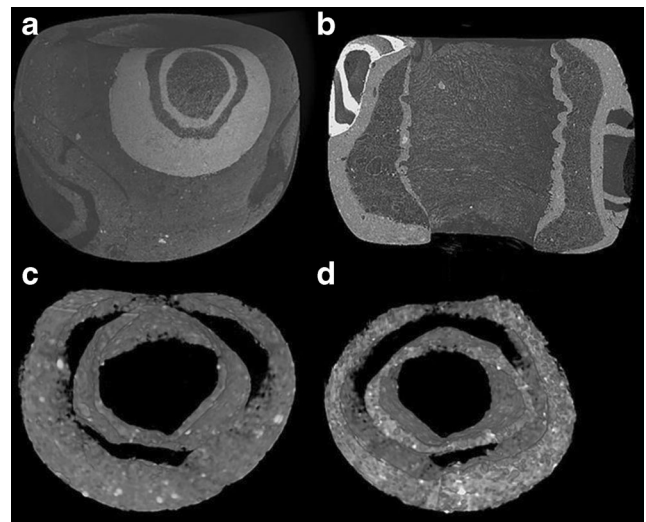
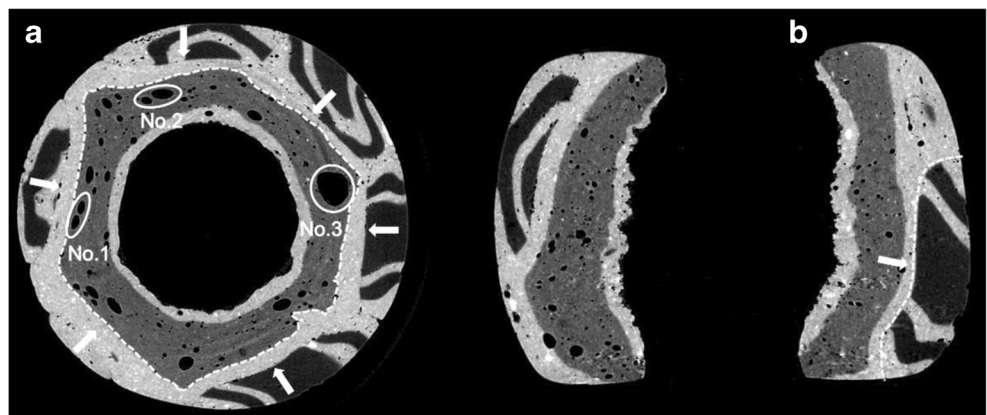
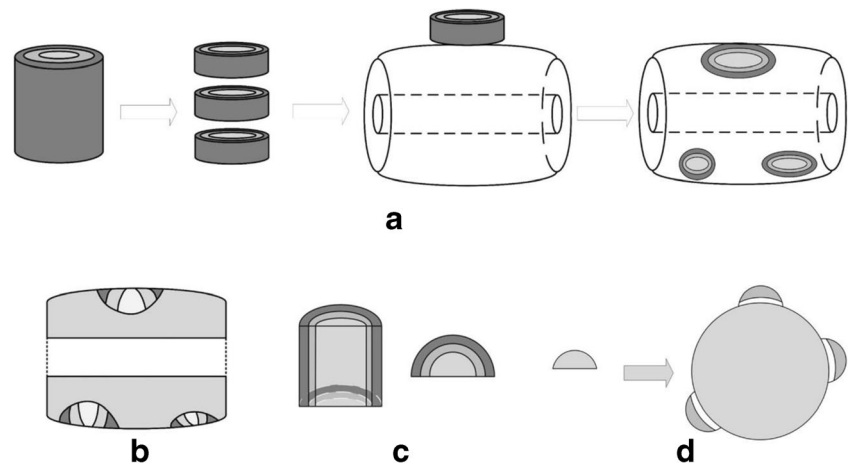


Fig. 5 The CT results of S-2. **a** The 3D diagram of S-2 and point out the location of the special eye (with highlight). **b** The longitudinal section of the glass bead. **c** The front view of extracted eye. **d** The back view of the extracted eye (The production process of eyes is shown through the method of density slicing)

at angles were evenly distributed between 0° and 180° . The exposure time per projection was 0.35 s. The total time of X-ray exposure was about 5 min for each CT scanning. As the samples were much bigger than the beam size at the vertical direction, a whole sample needed several CT scanning. After the acquisition, the dataset was reconstructed using the software PITRE (phase-sensitive X-ray image processing and tomography reconstruction). PITRE is a free software which can transform the projections to slices. It is developed by the staff of BL13W1 of SSRF. It was released since 2012 and no new version released up to now. Phase retrieval was carried out for each projection image, and then the tomographic slices were reconstructed using the filtered-back projection algorithm. The PITRE software (Chen et al. 2012:836e845) is to get the slices about samples, as well as the VG Studio max2.2 is the software about 3D reconstruction.

Fig. 6 **a** The manufacturing process of glass beads (The picture illustrates the production process of “eyes working.” It shows the cross sections of beads and the “eyes” structure.). **b** The longitudinal section of the glass bead. **c** The longitudinal and cross section of the “eye” before molding and cutting. **d** The manufacturing process of raised eyes (This process is guessed from the systematic research and published papers (Yang et al. 2013))



Results and discussions

Sample No. S-2

Figure 3 shows the picture and schematic representation of the sample S-2. In Fig. 4, there are two slices to show the cross section and the profile of the bead. It is interesting to find that a core of lower density exists inside the glass bead. The core is covered with a thick layer of white opaque glass which is consistent with the analytical findings. Even the inner wall of the hole is attached with a layer of the same white glass. In the results of CT scanning, the distinct colors represent different gray values and also correspond to the materials in different densities. Compared with core material, the glass layer shows the brighter appearance in the CT scanning images due to the higher density. Combined with the results of chemical composition, the brighter area indicates the white glaze contains $\text{Ca}_2\text{Sb}_2\text{O}_7$ as opacifier.

The figures illustrated that actually the base glass of the eye bead is nonhomogeneous glass. It is possible that an application glazing technique was used for the bead making. Although the body of the eye bead was covered with a quite thick layer of glaze, the manufacturing process may have been influenced by Faience making (Rehren 2008; Tite and Bimson 1986).

The core layer seems to present a porous material with many air bubbles in individual shapes. Normally, the air bubbles in glass or ceramic matrices were formed into standard spherical shapes during the vitrifying process. However, based on the shapes of the bubbles in Fig. 4, the arrows indicate the direction of pressure during the eye bead manufacturing. Under pressure, air bubbles No. 1 and No. 2 turn out to be elliptical because the direction of pressure is perpendicular to the macro axis of the ellipsoid (as shown by the arrows in Fig. 4a), which predict that the pressing happened when the eye slices were embedded into the base glass, and then force was transmitted to the core and deformed the shape of core bubbles. The arrows show the direction of force. There are six eyes in beads. So, there is a hexagon which indicates the force

from every side. The elliptical bubbles always located under the side of hexagon. The arrows and hexagon can be seen in Fig. 4a. While air bubble No. 3 deformed into an irregular circle created by force from two “eyes,” the irregular circle is always at the intersections of borders of hexagon. The kinds of pores (elliptical, spherical, irregular) can also see from other locations of air bubbles in Fig. 4a.

According to Fig. 4b, the boundary between the “eye” and “body” (arrow) is quite subtle because the base glass was also used to make the concentric ring of eye part. By analyzing the interlayered structures of the “eyes” shown by the slices, we know that the “eye” is made by materials of different densities (Fig. 5). The process of making “eyes” could be simply shown as in Fig. 6a–c, and the details of the production process could reconstruct as follows: a dark blue frit coated with

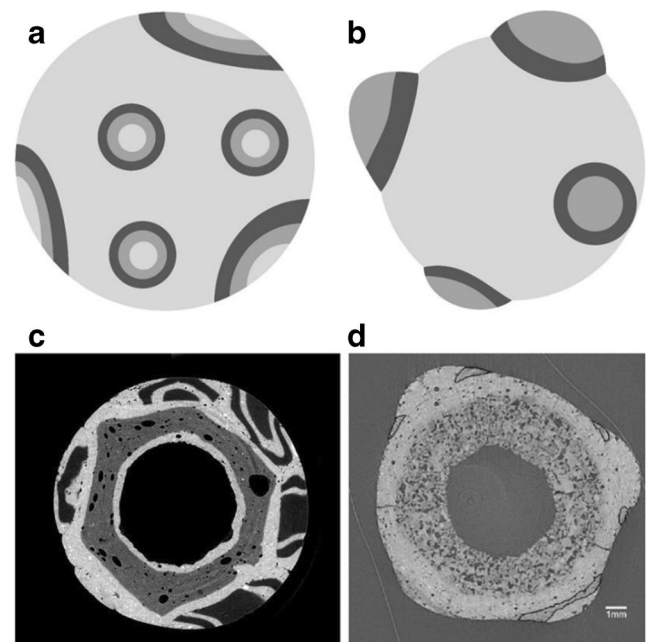


Fig. 7 **a** The embedded eye bead. **b** The raised eye bead. **c** The slice of embedded eye bead. **d** The slice of raised eye bead (This slice is from published papers—Yang et al. 2013)

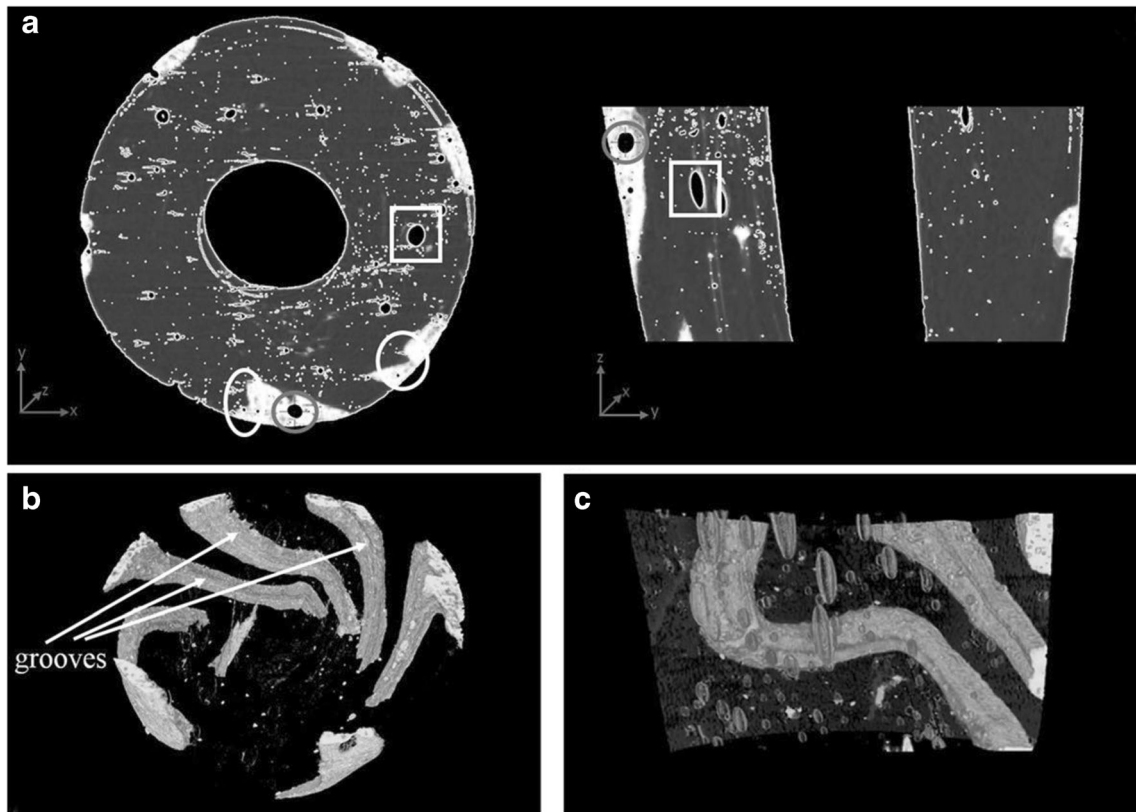


Fig. 8 **a** Different views of SC-8: the left slice is top view of SC-8 and the right is right view of SC-8. The two pictures show the bubbles in different areas of SC-8 (The gray circles show the stripe bubbles; the white square

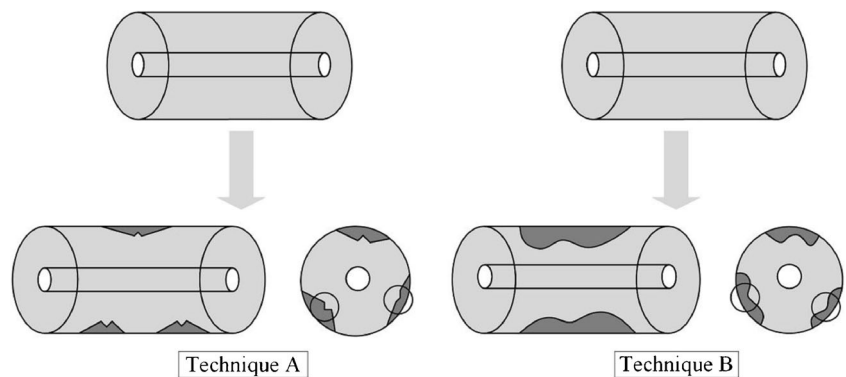
shows the based body bubbles and the white circles show the sharp corner of the stripes). **b** Stripes and **c** bubbles in the based body

glass in different colors formed a cane. The cane was cut into concentric rings slices in very thin layers. Eye slices were separately pressed into the base glass bead without any decoration under fusing condition.

The eye beads documented in China are divided into two types in terms of typology, the raised eye and the embedded eye (Fig. 7). The research of dragonfly eyes' technology, such as the analysis by Yang et al. (2013) for the raised eyes which were unearthed in Chu Tomb in Xichuan County of Henan Province. The slice is shown as Fig. 7d and the manufacturing

is shown as Fig. 6d. According to the research by Yang et al. (2013), the eye's working process could be described as follows: the quartz core was shaped as a spherical body, which would be glazed by the application method afterwards. Then, after firing, white ring glass was drawn on the glaze surface, and later horned eye cast in hemispherical molds were inlaid on the white rings. Compared with the manufacture of these two types of eye bead, it could be found that the embedded eye beads were made in the process of (semi)-melting molding and the raised eyes have a distinctly different process.

Fig. 9 The schematic drawings present stripes with different processes. Technique A: the stripes formed by melting glass filled in the groove. Technique B: the stripes applied to be embedded into the body



Sample No. SC-8

According to Fig. 8, we found that this bead was made into a spindle type. The blue base glass in Fig. 3 corresponds to SC-8 “body” (the following called based body), which shows a more compact body due to less air bubbles. The air bubbles in the body are mostly elliptical shape in the longitudinal section of the bead, while the yellow part in Fig. 3 corresponds to SC-8 “stripes.” In Fig. 8, the stripes are represented by the brighter area due to the existence of lead-tin yellow ($\text{Pb}_2\text{Sn}_2\text{O}_7$) glass as colorant. The chemical composition of the blue body and the yellow stripe shows they are typical plant ash soda-lime-silica glass.

By comparison with the blurred boundary between eye and body in sample S-2 (Fig. 4b), there are very clear connections between the stripes and body of SC-8 to form sharp corners (Fig. 8a). From the results of component analysis, the yellow stripes are shown as brighter colored areas on the CT scanning images. According to the longitudinal and cross section images of the yellow stripe, it is obvious that the yellow stripes have regular edges and sharp corners from Fig. 8b, c. It seems to indicate that small grooves had been carved around the blue raw glass before molten yellow glass was filled in.

In Fig. 8, the bubbles in the based body are elliptical in shape. The reasons are discussed here. First, during the glass-working process, the blue raw glass was stretched to form a spindle shape. When stretching, the round shape bubbles in the based body were also extended to elliptical shapes which can be seen from Fig. 8c. All of the air bubbles are elliptical shapes. Second, the bubbles in based body are standard ellipses, which indicate the SC-8 body has not suffered from extreme pressure. Because if there had been extra pressure to the body, the air bubbles would have become flat oval or irregular shapes. The bubbles in yellow stripes are still retained an intact spherical shape. This evidence suggests that there were no pressures and stretches; additionally, the embedding technique was not applied to the striped glass. Although some scholars have defined this type of ornamentation as a twisted color body, which should not have sharp edges or corners between each twisted color body’s layer during the working process (Fig. 9). This interpretation which suggests that the ornamentation was not embedded needs to be verified by further analysis of similar beads.

Therefore, the specific shapes of bubbles in based body and stripes seem to prove that molten yellow glass was applied into grooves probably carved by craftsman. This is a unique technique discovered by CT scanning. The manufacture of SC-8 combined with the method of stretching and carving. It is possible that this manufacturing approach was probably influenced by carving techniques for natural stone in the India-Pakistan region. In the further research, it should be compared with other bead making techniques by CT scanning.

Conclusion

Overall, by applying the CT scanning method, we could gain more valuable manufacturing information from the glass artifacts about the inner structure, materials distribution, bubble shape, and deformation.

The two glass beads discovered from Shanpula tomb site in ancient Khotan kingdom of Southern line of the Silk Road were analyzed and illustrated by CT scanning method. According to the chemical composition, eye bead S-2 is a typical soda-lime-silica glass using natron flux. However, the base part is inhomogeneous glass with a porous core extant inside. The manufacture seems to be influenced by the application technique of faience making. The “eyes” made by four concentric rings of glass materials were embedded into the base glass, based on shape analysis of the 3D image of the eyes and bubbles.

SC-8 is a soda-lime-silica glass bead with plant ash as flux, which is similar to beads discovered from Bara glass in Pakistan. The 3D view shows that the stripes of the bead have sharp edges, which implies carving of the body glass was done before the filling process. The elliptical bubbles in the turquoise body glass indicate the process of stretching technology. The intact spherical bubbles in stripes show that there was little pressure during the stripe decoration process. A natural assumption is that the carving technique probably imitated natural stone carving in India-Pakistan region.

The results of CT analysis of the two glass beads revealed the true structure of the eye bead and bubbles in different sections showing its use in deducing the possible manufacture. This research effectively shows how CT scanning is an advanced and nondestructive method to explore the anatomical structure of artifacts and obtain more valuable information which will contribute to understanding the materials and manufacturing.

Acknowledgements The authors would like to acknowledge the laboratory assistance of BL13W (SSRF, Shanghai, China) and would like to thank the National Nature Science Foundation of China (No. 31100680), the Joint Funds of the National Natural Science Foundation of China (No. U1232205), and the National Social Science Foundation of China (11CKG010) for the financial support. The authors would like to thank the Museum of Xinjiang Uygur Autonomous Region for providing the samples and the background information.

References

- Baruchel J, Buffiere JY, Cloetens P, di Michiel M, Ferrie E, Ludwig W, Maire E, Salvo L (2006) Advances in synchrotron radiation microtomography. *J Scr Mater* 55(1):41–46. <https://doi.org/10.1016/j.scriptamat.2006.02.012>
- Betz O et al (2007) Imaging applications of synchrotron X-ray phase-contrast micro-tomography in biological morphology and biomaterials science. I. General aspects of the technique and its advantages

- in the analysis of millimetre-sized arthropod structure. *J Microsc* 227(1):51–71. <https://doi.org/10.1111/j.1365-2818.2007.01785.x>
- Ferdinand von Richthofen (1877) *China: Ergebnisse Eigener Reisen Und Darauf Gegründeter Studien*. Berlin, pp 454
- Henderson J (1991) Chemical characterization of Roman glass vessels, enamels and tesserae. In: *Materials issues in art and archaeology II*, pp 601–607
- Jensen TH, Bech M, Bunk O, Thomsen M, Menzel A, Bouchet A, le Duc G, Feidenhans'l R, Pfeiffer F (2011) Brain tumor imaging using small-angle X-ray scattering tomography. *J Phys Med Biol* 56(6): 1717–1726. <https://doi.org/10.1088/0031-9155/56/6/012>
- Laure D, Bernard G (2013) Glass in South Asia, in: Koen H. A. Janssens (Eds.), *Modern methods for analysing archaeological and historical glass*. Wiley-Blackwell Publishing House, U.K., 399–411
- Meicun L (2006) *Fifteen lectures on archaeology of the silk roads*. Peking University Press, Beijing, 1–4
- Qian C (2017). The analytic report of “The origin and technology of glasses excavated in Shanpula cemetery, Khotan, Xinjiang Uyghur Autonomous Region.”, Beijing, Unpublished Report
- Rehren T (2008) A review of factors affecting the composition of early Egyptian glasses and faience: alkali and alkali earth oxides. *J Archaeol Sci* 35(5):1345–1354. <https://doi.org/10.1016/j.jas.2007.09.005>
- Rongchang C et al (2012) PITRE: software for phase-sensitive X-ray image processing and tomography reconstruction. *J Synchrotron Radiat* 19(5):836–845
- Shijie C et al (2013) Studying frozen soil with CT technology: present studies and prospects. *J Glaciol Geocryol* 35:193–200
- Tafforeau P, Boistel R, Boller E, Bravin A, Brunet M, Chaimanee Y, Cloetens P, Feist M, Hozowska J, Jaeger JJ, Kay RF, Lazzari V, Marivaux L, Nel A, Nemoz C, Thibault X, Vignaud P, Zabler S (2006) Applications of X-ray synchrotron micro-tomography for non-destructive 3D studies of paleontological specimens. *Appl Phys A Mater Sci Process* 83(2):195–202. <https://doi.org/10.1007/s00339-006-3507-2>
- Tite M, Bimson M (1986) Faience: an investigation of the microstructures associated with the different methods of glazing. *Archaeometry* 28(1):69–78. <https://doi.org/10.1111/j.1475-4754.1986.tb00375.x>
- Vicenzi et al (2002) Microbeam characterization of coming archaeological reference glasses: new additions to the Smithsonian microbeam standard collection. *J Res Natl Inst Stand Technol* 107(6):719–727. <https://doi.org/10.6028/jres.107.058>
- Xinjiang Museum, The Institute of Cultural Relic and Archaeology of Xinjiang (2001) *Shanpula of Xinjiang China—the open out and research of ancient Yutian civilization*. Xinjiang People's Publishing House, Xinjiang
- Yang Y, Wang L, Wei S, Song G, Kenoyer JM, Xiao T, Zhu J, Wang C (2013) Nondestructive analysis of dragonfly eye beads from the warring states period, excavated from a Chu tomb at the Shenmingpu site, Henan Province, China. *J Microsc Microanal* 19(02):335–343. <https://doi.org/10.1017/S1431927612014201>
- Yuqi R et al (2013) X-ray imaging and its biomedical applications at SSRF. *J. Chin. Bull Life Sci* 25:762–770